Published in final edited form as:
Cancer Res. 2010 June 1; 70(11): 4520–4527. doi:10.1158/0008-5472.CAN-09-4311.

Intratumoral therapy of glioblastoma multiforme using genetically engineered transferrin for drug delivery

Dennis J. Yoon[1], **Byron H. Kwan**[1], **Felix C. Chao**[1], **Theodore P. Nicolaides**[2], **Joanna J. Phillips**[3], **Gretchen Y. Lam**[1], **Anne B. Mason**[4], **William A. Weiss**[2], and **Daniel T. Kamei**[1,*]

[1]Department of Bioengineering, University of California, Los Angeles, CA 90095 U.S.A.

[2]Department of Neurology, Pediatrics, Neurological Surgery, and Brain Tumor Research Center, University of California, San Francisco, CA 94158 U.S.A.

[3]Department of Pathology, University of California, San Francisco, CA 94158 U.S.A.

[4]Department of Biochemistry, University of Vermont College of Medicine, Burlington, VT 05405 U.S.A.

Abstract

Glioblastoma multiforme (GBM) is the most common and lethal primary brain tumor with median survival of only 12-15 months under the current standard of care. To both increase tumor specificity and decrease nonspecific side effects, recent experimental strategies in the treatment of GBM have focused on targeting cell surface receptors, including the transferrin (Tf) receptor, that are overexpressed in many cancers. A major limitation of Tf-based therapeutics is the short association of Tf within the cell to deliver its payload. We previously developed two mutant Tf molecules, K206E/R632A Tf and K206E/K534A Tf, in which iron is locked into each of the two homologous lobes. Relative to wild-type Tf, we showed enhanced delivery of diphtheria toxin (DT) from these mutants to a monolayer culture of HeLa cells. Here, we extend the application of our Tf mutants to the treatment of GBM. *In vitro* treatment of Tf mutants to a monolayer culture of glioma cells demonstrated enhanced cellular association as well as enhanced delivery of conjugated DT. Treatment of GBM xenografts with mutant Tf conjugated DT resulted in pronounced regression *in vivo*, indicating their potential use as drug carriers.

Keywords

Transferrin; Diphtheria toxin; Glioblastoma multiforme; Mouse model; Targeted therapy

Introduction

Malignant gliomas are the most common primary brain tumor in the United States, accounting for 70% of the 21,810 estimated new cases of brain cancer in 2008 (1-3). Although the prevalence of malignant gliomas represents only 1.5% of the 1,437,180 new cancers diagnosed in 2008, glial tumors are associated with disproportionately high morbidity and mortality (1). For instance, grade IV astrocytomas, or glioblastoma multiforme (GBM), represent 60-70% of all malignant gliomas, with median survival of 12-15 months, despite administration of the current standard of care described below.

*Corresponding Author: Daniel T. Kamei, 5121 Engineering V, University of California, Los Angeles, CA 90095, Tel: (310) 206-4826, Fax: (310) 794-5956, kamei@seas.ucla.edu.

The first step in the treatment of malignant gliomas typically involves a gross surgical resection of the tumor (2). Next, to potentially eradicate residual cancer cells not surgically removed, the patient is given 6 weeks of radiation therapy (RT) concomitant with the chemotherapeutic temozolomide (TMZ). This treatment is followed by an additional 6 months of maintenance TMZ (4). Although this treatment regimen significantly increases the 1-3 month median survival of a patient newly diagnosed with GBM, there is much room for improvement. Possible reasons for the inability to extend survivability beyond ~1 year include the nonspecificity of RT and TMZ in combination with intrinsic cellular resistance to treatment (5,6) allowing GBM to recur after a median survival of 32-36 weeks (7). Consequently, a variety of agents have been investigated to combat GBM, many of which focus on proteins involved in the enhanced proliferative and migratory capacity characteristic of this disease (5,8-10). These approaches target proteins that are selectively expressed or overexpressed in tumors to minimize nonspecific toxicity to normal cells typical of conventional therapies.

Motivated by early clinical successes of GBM therapeutics, we undertook a study to improve upon the current standard of care utilizing the transferrin receptor (TfR) as our therapeutic target (11-13). Specifically, we were intrigued by Tf-CRM107, consisting of a human serum transferrin (Tf) molecule chemically conjugated to CRM107, a mutant variant of diphtheria toxin (DT). Though this conjugate drug had shown therapeutic promise in the treatment of progressive and recurrent GBM in both a Phase I and a multicenter Phase II study (5,6), a conditional power analysis in Phase III determined that Tf-CRM107 was unlikely to improve overall patient survival compared to the current standard of care (14). A reasonable hypothesis to account for this poor efficacy is the rapid cycling of Tf through the cell, severely limiting the time in which to deliver its toxin payload (15).

The trafficking pathway of Tf, by receptor-mediated endocytosis, serves the crucial physiological role of transporting iron to cells. Each Tf molecule is capable of binding two ferric (Fe^{3+}) ions, one in each of its two homologous iron binding lobes, the N-terminal lobe (N-lobe) and the C-terminal lobe (C-lobe) (16). Iron-loaded Tf (holo-Tf) specifically binds to TfR residing on the surface of all actively dividing cells. It is well known that many tumors significantly overexpress TfR relative to non-neoplastic tissue, ascribed to the extra need for iron of their rapidly proliferating cells (17,18). However, once Tf delivers its iron to the cell, iron-free Tf (apo-Tf) still bound to TfR is recycled to the cell surface, where it is released from its receptor; Tf cannot reenter cells until it acquires more iron, a rather inefficient process at this post-delivery site (13). Therefore, each holo-Tf molecule is restricted to a single 4-5 minute passage through the cell, while 30 such successive cycles of trafficking may be required for a Tf conjugated toxin to be delivered into the cytosol (19,20).

To enhance delivery of drugs conjugated to Tf, we developed a mathematical model describing the Tf/TfR trafficking pathway using the principles of mass action kinetics (15). A sensitivity analysis of the various model parameters identified decreasing the iron release rate in the endosome as a previously unreported design criterion to enhance the cellular association of Tf. By inhibiting the delivery of ferric ions by holo-Tf within the endosomal compartment, we manipulated the cell to recycle holo-Tf, rather than apo-Tf, to the cell surface. Each Tf molecule can now cycle through its trafficking pathway multiple times, since holo-Tf maintains a high affinity for TfR at the cell surface and could reenter the cell, increasing the probability that a Tf conjugated toxin will deliver its cytotoxic payload. Recombinant protein technology was used to develop two mutant variants of Tf exhibiting reduced iron release kinetics (21,22). Both mutants contain two point mutations, one within each iron binding lobe specifically targeting amino acids involved in the release of iron within the endosomal compartment. *In vitro* studies with HeLa cervical cancer cells displayed significantly higher drug delivery efficacy by both mutant Tf proteins in comparison to the wild-type Tf control (23).

Here we utilized these mutant Tf-DT conjugates in the treatment of GBM. *In vitro* studies with the U87 and U251 glioblastoma cell lines demonstrated increased drug delivery efficacy attributed to the mutant Tf proteins. Moreover, application of mutant Tf-DT conjugates to xenografted U87:*EGFRvIII* flank tumors demonstrated superior and rapid tumor regression when compared with wild-type Tf-DT controls. These results establish the potential for clinical application of mutant Tf-based therapeutics in the treatment of malignant gliomas.

Materials and Methods

Cell Culture

U251 glioma cells were a kind gift from Dr. Robert M. Prins and Dr. Linda M. Liau (UCLA Neurosurgery, Los Angeles, CA). U87 glioma cells were purchased from the American Type Culture Collection (ATCC, Manassas, VA). Both cell types were seeded on 75 cm^2 tissue culture flasks (Corning Incorporated, Corning, NY) and grown in Dulbecco's Modified Eagle Medium supplemented with high glucose (DMEM-HG; Invitrogen, Carlsbad, CA) with 3.6 g/L sodium bicarbonate, 10% fetal bovine serum (Hyclone, Logan, UT), 1 mM sodium pyruvate, 100 units/mL penicillin (Invitrogen) and 100 μg/mL streptomycin (Invitrogen) at a pH of 7.4 (growth medium). The cells were incubated in a humidified atmosphere with 5% CO_2 at 37° C. For *in vivo* use, U87 cells were transduced with a retroviral-based pLRNL-neo-EGFRvIII plasmid, kindly provided by Dr. Russ Pieper (UCSF Neurological Surgery, Brain Tumor Research Center, San Francisco, CA), as previously described (24). Authentication on all cell lines used in this study was performed using the Promega Powerplex® 1.2 system (Promega, Madison, WI) for STR analysis as recommended by ATCC. Results indicate that the cell lines used in this study are authentic. All reagents and materials were purchased from Sigma-Aldrich (St. Louis, MO) unless otherwise specified.

Production of Recombinant Tf Expression Vectors

Recombinant Tf mutants were generated via site-directed mutagenesis introduced into the pNUT N-His K206E hTf NG construct using the QuickChange mutagenesis kit (Stratagene, La Jolla, CA) as described previously (21). Mutations of residues in the C-lobe, Arg 632 and Lys 534 to alanine, were introduced into the plasmid already containing the N-lobe mutation, K206E, by PCR using two sets of complimentary mutagenic oligonucleotide primers. Another plasmid coding for the N-terminal hexa His-tagged nonglycosylated recombinant Tf (wild-type Tf) served as a control (25).

Production and Purification of Recombinant Tf

The recombinant Tf plasmids were transfected into baby hamster kidney (BHK) cells for protein expression. The recombinant proteins are secreted into the tissue culture medium (25). Conversion of all recombinant Tf to the fully (and most stable) ferric form involved addition of Fe-NTA to the tissue culture medium. Purification was accomplished by chromatography on a Ni-NTA column (Qiagen Incorporated, Valencia, CA) using a BioCad Sprint chromatography system. A Sephacryl S200HR gel filtration column was used as the final step of purification, fully exchanging the proteins into 100 mM NH_4HCO_3. The samples were stored at -20°C as concentrated stock solutions (~2.5 mM) (26).

Radioiodination of Recombinant Tf

Holo-Tf samples were specifically radiolabeled at tyrosine residues with $Na^{125}I$ purchased from MP Biomedicals (Irvine, CA) using IODO-BEADS (Pierce Biotechnology, Rockford, IL). Size exclusion chromatography through Sephadex G10 columns was used to eliminate free ^{125}I from the labeled protein. The specific activity and concentration of each radioiodinated

holo-Tf was determined by a phosphotungstic acid assay. The labeled protein was used in Tf/TfR cellular trafficking studies.

Tf/TfR Cellular Trafficking Studies

U251 and U87 glioma cells were seeded in growth medium onto 35 mm dishes (Becton Dickinson and Company, Franklin Lakes, NJ) at a density of 3.0×10^4 cells/cm^2 and 4.0×10^4 cells/cm^2, respectively. Different seeding densities were used due to differences in both the size and the proliferative rate of the cells. Following an incubation period of 14-16 h in a humidified 5% CO_2, 37°C environment, the growth medium was aspirated, and incubation medium (DMEM-HG, 20 mM HEPES, 1 mM sodium pyruvate, 100 units/mL penicillin, 100 μg/mL streptomycin and 1 g/L bovine serum albumin, pH 7.4) containing 1 nM of radioiodinated Tf was added to each dish. The cells were then placed in a 37°C environment for 5, 15, 30, 60, 90, and 120 min after which the incubation medium was removed. The cells were washed five times with ice-cold WHIPS (20 mM HEPES, 1 g/L polyvinylpyrrolidone, 130 mM NaCl, 5 mM KCl, 0.5 mM $MgCl_2$ and 1 mM $CaCl_2$, pH 7.4) to remove nonspecifically bound ligand. To separate cell surface Tf specifically bound to TfR from internalized Tf, 1 mL of ice-cold acid strip (50 mM glycine-HCl, 100 mM NaCl, 1 g/L polyvinylpyrrolidone and 2 M urea, pH 3.0) was added to each dish and then placed on ice for 12 min. Each dish was washed once more with 1 mL acid strip. The cells were solubilized by adding 1 mL of 1 N NaOH to each dish for 30 min followed by an additional wash with 1 mL of 1 N NaOH. The two basic washes were collected, and the solution was assayed for radioactivity using a Cobra Series Auto-Gamma Counter (Packard Instrument Co., Meriden, CT) to determine the amount of internalized ligand. Experiments were performed three times with triplicate time points for each Tf ligand.

Conjugation of Recombinant Tf to DT

DT conjugates of recombinant Tf were prepared using the chemical crosslinkers 2-iminothiolane (2-IT) and N-succinimidyl 3-(2-pyridyldithio) propionate (SPDP), purchased from Pierce, to create a reducible disulfide bond. DT in PBS was thiolated with an 8-fold molar excess of 2-IT for 60 min at room temperature. The thiolated DT was separated from free 2-IT by size exclusion chromatography using Zeba desalting spin columns (Pierce). Recombinant Tf in PBS was reacted with a 3-fold molar excess of SPDP for 30 min at room temperature. This SPDP modified Tf (Tf-SPDP) compound was separated from free SPDP by size exclusion chromatography using Zeba desalting spin columns. Tf-SPDP and thiolated DT (1:1 molar ratio) were mixed, diluted and incubated overnight at 4°C. Tf-DT conjugates were purified by HPLC (AKTA FPLC Chromatographic Systems, GE Healthcare Bio-Sciences, Piscataway, NJ) using two HiPrep 16/60 Sephacryl S200HR size exclusion columns in series (GE Healthcare). The identity of each peak was confirmed with SDS-PAGE, and the concentration of the 1:1 Tf-DT conjugates was quantified using the Bradford dye binding assay.

In Vitro Cytotoxicity Studies

The sulforhodamine B (SRB) cell proliferation assay was used to quantify cell survival based on the measurement of cellular protein content (27). U251 and U87 glioma cells were seeded onto each well of a 96-well tissue culture plate at cell densities of 1.5×10^4 cells/cm^2 and 3.0×10^4 cells/cm^2, respectively. As mentioned above, different seeding densities were used due to differences in the cell sizes and their proliferation rates. After overnight incubation, growth medium was aspirated, and the cells were incubated for 48 h with 100 μL of fresh growth medium containing concentrations of Tf-DT spanning three orders of magnitude (10^{-4} to 10^{-1} nM). Then, 100 μL of cold 10% trichloroacetic acid (TCA) was added to each well to fix the cells at 4°C for 1 h. The TCA solution was removed, and the cells were washed four times with distilled water then thoroughly blow-dried. Subsequently, 50 μL of a 1% acetic

acid solution containing 0.4% SRB was added to each well for 30 min at room temperature. The dye solution was removed, and the cells were washed four times with a 1% acetic acid solution to remove unbound dye; following this step the cells were again blow-dried. The dye was dissociated from the proteins and solubilized with 100 μL of a 10 mM Tris base solution. The absorbance of each well was determined with an Infinite F200 plate reader (Tecan Systems Incorporated, San Jose, CA) at wavelengths of 560 nm and 700 nm. The survival of cells relative to a control (*i.e.* cells incubated in growth medium without Tf-DT) was calculated by determining the ratio of the ($A_{560} - A_{700}$) values. Experiments were performed three times with quadruplicate points per each concentration.

Intratumoral therapy of mice with glioma flank tumors

The treatment regimen presented here was modeled after the methods developed by Oldfield and coworkers for Tf-CRM107 (28). Solid U87:*EGFRvIII* glioma flank tumors were established in 4-6 week old *nu/nu* female mice by subcutaneous injection of 5×10^6 cells. This cell line expresses *EGFRvIII*, a constitutively active mutant variant of EGFR, which leads to more rapid proliferation than the typical U87 cell line (9), allowing palpable tumors of 0.5 cm in diameter to be established in a relatively short period of 2 weeks. Flank tumors were established on both flanks of mice to maximize mouse usage. Each mouse participated in only one treatment cohort, eliminating the possibility of any systemic effect on the contralateral tumor. Once tumors reached volumes of 200 mm^3, they were randomly assigned into one of four treatment groups, each containing four tumors. Each tumor received a 100 μL intratumoral injection of PBS containing no drug (the control) or 0.25 μg of one of the Tf-DT samples. The injections occurred every other day starting at day 0 and ending on day 6. Following the 6^{th} day, no further injections were given, and the tumor volume was continuously measured for a period of 4 weeks or until the mice were sacrificed due to excessive tumor growth. Tumor measurements were performed using calipers, and tumor volumes were calculated using the ellipsoid formula $\frac{1}{2}(LW^2)$, where L equals length (longest diameter) and W equals width (widest part of tumor perpendicular to L). Monitoring was performed to observe a continued regression of the tumor, a plateau in tumor size, or tumor recurrence. All mouse experiments were performed in accordance with the Institutional Animal Use Committee at UCSF.

Histology and immunohistochemistry

Additional U87:*EGFRvIII* flank tumors were generated and used for histology. Subcutaneous tumors were grown to volumes of 200 mm^3 and treated intratumorally with 2 doses (on day 0 and day 2) with either PBS or Tf-DT. Mice were sacrificed and flank tumors removed 24 h post-treatment. Tumors were routinely fixed in phosphate-buffered 4% formalin, dehydrated by graded ethanols, and embedded in Paraplast Plus wax (McCormick Scientific, St. Louis, MO). Fixed tumors were treated with a solution containing 0.8 μg/mL rabbit polyclonal cleaved caspase-3 antibody (Cell Signaling Technology, Danvers, MA) for 32 min at 37°C. Antigen retrieval for cleaved caspase-3 was performed for 8 min in Tris buffer (pH 8) at 90°C. Sections were subsequently treated with a 3% methanol-hydrogen peroxide solution at 22°C for 16 min. Nuclei were counterstained with hematoxylin. All immunohistochemistry (IHC) assays were performed on the Benchmark XT (Ventana Medical Systems Inc, Tucson, AZ) using the iView detection system. Slides stained for cleaved caspase-3 were scored based on the percentage of tumor cells that stained positive. A score of 0, 1, 2, or 3 denoted that 0%, 1-5%, 6-25% or >25% of tumor cells stained positive for cleaved caspase-3, respectively.

Results

Mutant Tf shows increased association with glioma cells

The engineered ligands, K206E/R632A Tf and K206E/K534A Tf, with a significantly increased ability to retain iron relative to wild-type Tf, were found to have an increased cellular

association in a HeLa cell system (23). To determine whether these mutants showed similar increased cellular association in glioma cells, we measured the concentration of internalized Tf in U251 and U87 glioma cells over time and evaluated the cumulative exposure of cells to a Tf conjugated drug as determined by area under the curve (AUC) analysis. At the end of the 2 h incubation period, the internalized level of wild-type Tf in U251 cells was 2.29×10^4 molecules/cell compared to values of 4.77×10^4 and 7.26×10^4 molecules/cell for K206E/R632A Tf and K206E/K534A Tf, respectively. AUC values were 2.29×10^6, 3.48×10^6 and 5.17×10^6 (#·min)/cell for wild-type Tf, K206E/R632A Tf and K206E/K534A Tf, respectively (figure 1A). These values translate into an AUC increase of 54.7% and 147% over the wild type. This trend in AUC increase was confirmed by two additional experiments yielding average AUC values of $(2.75 \pm 0.41) \times10^6$ (#·min)/cell for wild-type Tf compared to values of $(4.15 \pm 0.65) \times10^6$ ($p = 0.0173$) and $(6.67 \pm 1.32) \times10^6$ (#·min)/cell ($p = 0.0039$) for K206E/R632A Tf and K206E/K534A Tf, respectively, which translate to AUC increases of $50.5 \pm 23.4\%$ and $142 \pm 48\%$. The student t-test was used to show that the increase in AUC exhibited by each mutant Tf compared to wild type was statistically significant ($p < 0.05$).

Comparable results were obtained using U87 cells (figure 1B). At the end of the 2 h incubation period, the internalization level of wild-type Tf was 2.87×10^4 molecules/cell compared to values of 7.04×10^4 and 11.8×10^4 molecules/cell for K206E/R632A Tf and K206E/K534A Tf, respectively. AUC values were 2.95×10^6, 4.97×10^6 and 8.43×10^6 (#·min)/cell for wild-type Tf, K206E/R632A Tf and K206E/K534A Tf, respectively. This translates into AUC increases of 68.4% and 186%. This trend was confirmed by two additional experiments yielding average AUC values of $(2.50 \pm 0.68) \times 10^6$ (#·min)/cell for wild-type Tf compared to values of $(4.04 \pm 0.92) \times 10^6$ ($p = 0.0396$) and $(6.81 \pm 1.41) \times 10^6$ (#·min)/cell ($p = 0.0044$) for K206E/R632A Tf and K206E/K534A Tf, respectively, which translate to AUC increases of $61.5 \pm 36.7\%$ and $172 \pm 56\%$.

In Vitro Toxicity of Tf-DT

Having confirmed the increased association of the recombinant mutant Tf with glioma cells compared to wild-type Tf, we next evaluated the *in vitro* efficacy of drug delivery to glioma cells. We synthesized and administered DT conjugates of the various Tf ligands to U251 and U87 cells over a range of concentrations for 48 h. Each mutant Tf-DT exhibited significantly enhanced drug delivery efficacy relative to wild-type Tf-DT (figure 2). Figures 2A and 2B correspond to the cytotoxic effects of Tf-DT conjugates against the U251 glioma cell line, indicating that less drug is required for the mutant conjugate to achieve the same level of cytotoxicity in comparison to the wild-type conjugate. IC_{50} values, or the concentrations at which 50% inhibition of cellular growth occurs, were 9.70 ± 0.50 pM for wild-type Tf versus 6.94 ± 0.52 pM ($p = 0.001$) and 6.47 ± 0.76 pM ($p = 0.002$) for K206E/R623A Tf and K206E/K534A Tf, respectively. As shown in figures 2C and 2D, the same trend was observed with U87 cells, demonstrating IC_{50} values of 15.0 ± 3.00 pM for wild-type Tf compared to values of 7.85 ± 1.55 pM ($p = 0.01$) and 6.82 ± 1.21 pM ($p = 0.006$) for K206E/R632A Tf and K206E/K534A Tf, respectively. The student t-test was used to show that the decrease in IC_{50} exhibited by both mutant Tf-DT conjugates compared to the wild-type counterpart was statistically significant ($p < 0.05$).

In vivo efficacy and safety of Tf-DT delivered systemically to mice

To determine whether this *in vitro* efficacy of our novel Tf-based conjugates could be observed *in vivo*, we applied our conjugates to mice with established subcutaneous glioma flank tumors. Consistent with the data obtained in figure 2, the mutant Tf-DT conjugates show a significant improvement in reducing tumor bulk in flank xenografts (figure 3). The results for the tumors treated with the PBS control show rapid tumor growth due to a lack of drug treatment. Therefore, the mice with these tumors were prematurely sacrificed, and consequently, data for

these tumors did not extend beyond day 8. The results for the tumors treated with the wild-type Tf-DT demonstrate a delayed growth profile. However, the data for the average of four tumors treated with this cohort display a very large standard deviation. The reason for this behavior is that, while two of the tumors in this treatment group displayed a delayed growth profile similar to the averaged curve, the growth of the other two tumors in the wild-type group was suppressed with evidence of tumor regression near the final days of the observation period. Though the reasons for this inconsistency are unclear at this time, it is apparent that, at the dosage used, the two mutant Tf-DT conjugates outperformed the wild-type Tf-DT. For each mutant Tf-DT, rapid and near complete tumor regression was observed in all four tumors. Mice were examined and weighed daily. All mice continued to gain weight at an equal rate throughout the treatment regardless of treatment cohort (data not shown), suggesting that tumor apoptosis was a specific effect of Tf-DT therapy, and not a result of systemic toxicity.

DT conjugates induce apoptosis in U87:*EGFRvIII* xenografts

Following the above *in vivo* treatment and observation protocol, additional tumors were treated with two doses of each therapy. Mice were sacrificed 24 h post-treatment and tumors harvested for histological and IHC analyses. IHC analysis for expression levels of cleaved caspase-3 (figure 4) verified that toxin conjugate treatment decreased tumor growth through an increase in apoptosis. U87:*EGFRvIII* flank tumors showed little baseline apoptosis (figure 4A) demonstrating low cleaved caspase-3 levels with an immunostain score of 0. The wild-type Tf-DT induced a moderate level of apoptosis (figure 4B) with an immunostain score between 1 and 2. Tumors treated with either mutant Tf-DT demonstrated the greatest level of apoptosis (figure 4C and 4D) with immunostain scores of 3.

Discussion

TfR has been a cancer cell target of interest for many years because of its naturally high expression in cancer cells. Both monoclonal antibodies (mAbs) to TfR and the Tf ligand itself have been utilized to selectively target therapies to tumors while minimizing toxicities toward non-neoplastic cells and tissue (29). In some cases, use of Tf mAb-based conjugates was preferred over Tf-based conjugates, since (i) Tf only has a short period of time to deliver its payload and (ii) high endogenous levels of Tf may prevent the Tf-drug conjugates from reaching cancer cells (30). However, other studies have found that the alternative trafficking behavior of Tf mAb-based conjugates, which appear to be targeted to the lysosome for degradation rather than following the conventional recycling pathway, may adversely influence the effectiveness of protein drugs such as DT and CRM107 (15).

Recently, we identified a novel design strategy to increase the time Tf spends inside a cancer cell. Through the aid of a mathematical model of the Tf/TfR trafficking pathway, we determined that decreasing the iron release kinetics of Tf in the acidic endosome is an effective means of increasing the drug delivery efficacy of Tf. With knowledge gained from recent work regarding the mechanism of iron release within the Tf/TfR cell cycle (16,21,22,25,26), we used site-directed mutagenesis to generate two mutants of Tf, K206E/R632A Tf and K206E/K534A Tf. These mutations were highly effective in decreasing Tf iron release within the acidic endosomal compartment (31); each mutant possesses a single point mutation in each of the two lobes which effectively blocks or drastically slows iron release from either lobe.

The K206E mutation comprises one half of a motif in the N-lobe known as the *dilysine trigger* (22,32). The dilysine trigger is comprised of two lysine residues, K206 and K296, which facilitate the release of iron at the acidic pH of the endosome. By converting lysine at position 206 to glutamate, iron removal from this lobe is significantly inhibited by formation of a salt bridge between the negatively charged Glu206 on one side of the binding cleft and the positively charged Lys296 on the other side. In a similar fashion, iron release from the C-lobe

is influenced by a *pH sensitive triad* comprised of three amino acid residues, Lys534, Arg632, and Asp634 (21). Alanine scanning revealed that substitution of an alanine residue to either Lys534 or Arg632 significantly inhibited iron removal from the C-lobe.

We therefore generated K206E/R632A Tf and K206E/K534A Tf and subjected these mutants to *in vitro* drug delivery efficacy studies in HeLa cells. This study provided proof-of-principle that manipulation of Tf was an effective means of altering its drug delivery efficacy and thereby helped to circumvent the problem of the short association time of wild-type Tf within cells. The study presented here substantiates this finding and extends the applicability of our approach *in vitro* to a second tumor type, GBM, and further translates these *in vitro* results into glioma xenograft models *in vivo*.

The restricted nature of GBM within the brain cavity confines it to a region of generally low TfR expression separated from systemic circulation via the largely impregnable blood-brain barrier (BBB) (33,34). Though this permits the possibility of specifically targeting DT to neoplastic tissue while minimizing toxicities toward normal brain tissue, the BBB along with high endogenous levels of Tf precludes the intravenous application of Tf-DT. To address these issues, we intend to administer the mutant Tf-DT conjugates locally in the treatment of GBM. Although systemic therapies are generally preferred, the current treatment of GBM already involves an invasive surgical resection procedure; therefore, patients with GBM are expected to be more open to local therapies, as suggested by the clinical trials of Tf-CRM107. Moreover, direct application allows for on-site tumor delivery of therapeutics in high concentrations and effectively provides the therapeutic agent immediate access to the tumor site. For example, convection enhanced delivery, or CED, can be used for the direct application of our novel therapeutic, as in the case of Tf-CRM107 (6), where convective mass transfer facilitates intratumoral drug distribution over a larger tumor volume enhancing its tumor accessibility (35,36). In this scenario, the high endogenous Tf concentration is a desirable feature, since any mutant Tf-DT conjugates that diffuse away from the tumor site and into systemic circulation would be outcompeted by endogenous Tf for available receptor sites on normal tissue.

The earlier success of Tf-CRM107 in Phase II clinical trials, in which the conjugate was well tolerated by patients with GBM, indicates that clinical potential exists for the mutant Tf-toxin conjugates described in this study. Though Phase III trials of Tf-CRM107 were halted based on a conditional power analysis predicting less efficacy than the current standard of care, our mutant Tf-based conjugates show an improved therapeutic efficacy that may warrant support for continued clinical investigation of Tf as a drug carrier against GBM.

Acknowledgments

This work was funded by the Wallace H. Coulter Foundation Early Career Award and the Cancer Research Coordinating Committee grant to D.T.K., USPHS grant R01 DK 21739 to A.B.M, the Burroughs Wellcome Fund, Brain Tumor Society, Accelerate Brain Cancer Cure, Samuel G. Waxman Foundation and NIH P50CA097257 to W.A.W, and the Campini Foundation, American Brain Tumor Association and NIH T32 CA108462-01 to T.P.N. The authors thank Dr. Robert M. Prins and Dr. Linda M. Liau, Department of Neurosurgery, UCLA, for kindly providing the U251 cells, and Dr. Russ Pieper, UCSF Neurological Surgery and Brain Tumor Research Center, for kindly providing the retroviral-based pLRNL-neo-EGFRvIII plasmid.

References

1. Wen PY, Kesari S. Malignant gliomas in adults. The New England journal of medicine 2008;359:492–507. [PubMed: 18669428]
2. Welch M, Lai R. Glioblastoma multiforme. Current treatment options in neurology 2009;11:297–305. [PubMed: 19523355]
3. Jemal A, Siegel R, Ward E, et al. Cancer statistics, 2008. CA: a cancer journal for clinicians 2008;58:71–96. [PubMed: 18287387]

4. Stupp R, Mason WP, van den Bent MJ, et al. Radiotherapy plus concomitant and adjuvant temozolomide for glioblastoma. The New England journal of medicine 2005;352:987–96. [PubMed: 15758009]
5. Weaver M, Laske DW. Transferrin receptor ligand-targeted toxin conjugate (Tf-CRM107) for therapy of malignant gliomas. Journal of neuro-oncology 2003;65:3–13. [PubMed: 14649881]
6. Laske DW, Youle RJ, Oldfield EH. Tumor regression with regional distribution of the targeted toxin TF-CRM107 in patients with malignant brain tumors. Nature medicine 1997;3:1362–8.
7. Hou LC, Veeravagu A, Hsu AR, Tse VC. Recurrent glioblastoma multiforme: a review of natural history and management options. Neurosurgical focus 2006;20:E5. [PubMed: 16709036]
8. Morokoff AP, Novak U. Targeted therapy for malignant gliomas. J Clin Neurosci 2004;11:807–18. [PubMed: 15519855]
9. Sampson JH, Archer GE, Mitchell DA, Heimberger AB, Bigner DD. Tumor-specific immunotherapy targeting the EGFRvIII mutation in patients with malignant glioma. Seminars in immunology 2008;20:267–75. [PubMed: 18539480]
10. Reardon DA, Akabani G, Coleman RE, et al. Phase II trial of murine (131)I-labeled antitenascin monoclonal antibody 81C6 administered into surgically created resection cavities of patients with newly diagnosed malignant gliomas. J Clin Oncol 2002;20:1389–97. [PubMed: 11870184]
11. Gatter KC, Brown G, Trowbridge IS, Woolston RE, Mason DY. Transferrin receptors in human tissues: their distribution and possible clinical relevance. Journal of clinical pathology 1983;36:539–45. [PubMed: 6302135]
12. Niitsu Y, Kohgo Y, Nishisato T, et al. Transferrin receptors in human cancerous tissues. The Tohoku journal of experimental medicine 1987;153:239–43. [PubMed: 3433281]
13. Qian ZM, Li H, Sun H, Ho K. Targeted drug delivery via the transferrin receptor-mediated endocytosis pathway. Pharmacological reviews 2002;54:561–87. [PubMed: 12429868]
14. Debinski W. Molecular targeting with recombinant cytotoxins for the treatment of brain tumors. Drug Development Research 2008;69:407–14.
15. Lao BJ, Tsai WL, Mashayekhi F, Pham EA, Mason AB, Kamei DT. Inhibition of transferrin iron release increases in vitro drug carrier efficacy. J Control Release 2007;117:403–12. [PubMed: 17239470]
16. Lin LN, Mason AB, Woodworth RC, Brandts JF. Calorimetric studies of the binding of ferric ions to human serum transferrin. Biochemistry 1993;32:9398–406. [PubMed: 8369310]
17. Ponka P, Lok CN. The transferrin receptor: role in health and disease. The international journal of biochemistry & cell biology 1999;31:1111–37.
18. Cazzola M, Bergamaschi G, Dezza L, Arosio P. Manipulations of cellular iron metabolism for modulating normal and malignant cell proliferation: achievements and prospects. Blood 1990;75:1903–19. [PubMed: 2186818]
19. Klausner RD, Van Renswoude J, Ashwell G, et al. Receptor-mediated endocytosis of transferrin in K562 cells. The Journal of biological chemistry 1983;258:4715–24. [PubMed: 6300098]
20. Johnson VG, Wilson D, Greenfield L, Youle RJ. The role of the diphtheria toxin receptor in cytosol translocation. The Journal of biological chemistry 1988;263:1295–300. [PubMed: 3257214]
21. Halbrooks PJ, He QY, Briggs SK, et al. Investigation of the mechanism of iron release from the C-lobe of human serum transferrin: mutational analysis of the role of a pH sensitive triad. Biochemistry 2003;42:3701–7. [PubMed: 12667060]
22. He QY, Mason AB, Tam BM, MacGillivray RT, Woodworth RC. Dual role of Lys206-Lys296 interaction in human transferrin N-lobe: iron-release trigger and anion-binding site. Biochemistry 1999;38:9704–11. [PubMed: 10423249]
23. Yoon DJ, Chu DS, Ng CW, et al. Genetically engineering transferrin to improve its in vitro ability to deliver cytotoxins. J Control Release 2009;133:178–84. [PubMed: 18992290]
24. Fan QW, Weiss WA. RNA interference against a glioma-derived allele of EGFR induces blockade at G2M. Oncogene 2005;24:829–37. [PubMed: 15580296]
25. Mason AB, He QY, Halbrooks PJ, et al. Differential effect of a his tag at the N- and C-termini: functional studies with recombinant human serum transferrin. Biochemistry 2002;41:9448–54. [PubMed: 12135367]

26. Mason AB, He QY, Adams TE, et al. Expression, purification, and characterization of recombinant nonglycosylated human serum transferrin containing a C-terminal hexahistidine tag. Protein expression and purification 2001;23:142–50. [PubMed: 11570856]
27. Skehan P, Storeng R, Scudiero D, et al. New colorimetric cytotoxicity assay for anticancer-drug screening. Journal of the National Cancer Institute 1990;82:1107–12. [PubMed: 2359136]
28. Laske DW, Ilercil O, Akbasak A, Youle RJ, Oldfield EH. Efficacy of direct intratumoral therapy with targeted protein toxins for solid human gliomas in nude mice. Journal of neurosurgery 1994;80:520–6. [PubMed: 8113865]
29. Yazdi PT, Murphy RM. Quantitative analysis of protein synthesis inhibition by transferrin-toxin conjugates. Cancer research 1994;54:6387–94. [PubMed: 7987833]
30. Gosselaar PH, van-Dijk AJG, de-Gast GC, et al. Transferrin toxin but not transferrin receptor immunotoxin is influenced by free transferrin and iron saturation. Euro J Clin Invest 2002;32:61–9.
31. Byrne SL, Mason AB. Human serum transferrin: a tale of two lobes. Urea gel and steady state fluorescence analysis of recombinant transferrins as a function of pH, time, and the soluble portion of the transferrin receptor J Biol Inorg Chem 2009;14:771–81.
32. MacGillivray RT, Moore SA, Chen J, et al. Two high-resolution crystal structures of the recombinant N-lobe of human transferrin reveal a structural change implicated in iron release. Biochemistry 1998;37:7919–28. [PubMed: 9609685]
33. Angelova-Gateva P. Iron transferrin receptors in rat and human cerebrum. Agressologie: revue internationale de physio-biologie et de pharmacologie appliquees aux effets de l'agression 1980;21:27–30.
34. Jefferies WA, Brandon MR, Hunt SV, Williams AF, Gatter KC, Mason DY. Transferrin receptor on endothelium of brain capillaries. Nature 1984;312:162–3. [PubMed: 6095085]
35. Bobo RH, Laske DW, Akbasak A, Morrison PF, Dedrick RL, Oldfield EH. Convection-enhanced delivery of macromolecules in the brain. Proceedings of the National Academy of Sciences of the United States of America 1994;91:2076–80. [PubMed: 8134351]
36. Bidros DS, Vogelbaum MA. Novel drug delivery strategies in neuro-oncology. Neurotherapeutics 2009;6:539–46. [PubMed: 19560743]

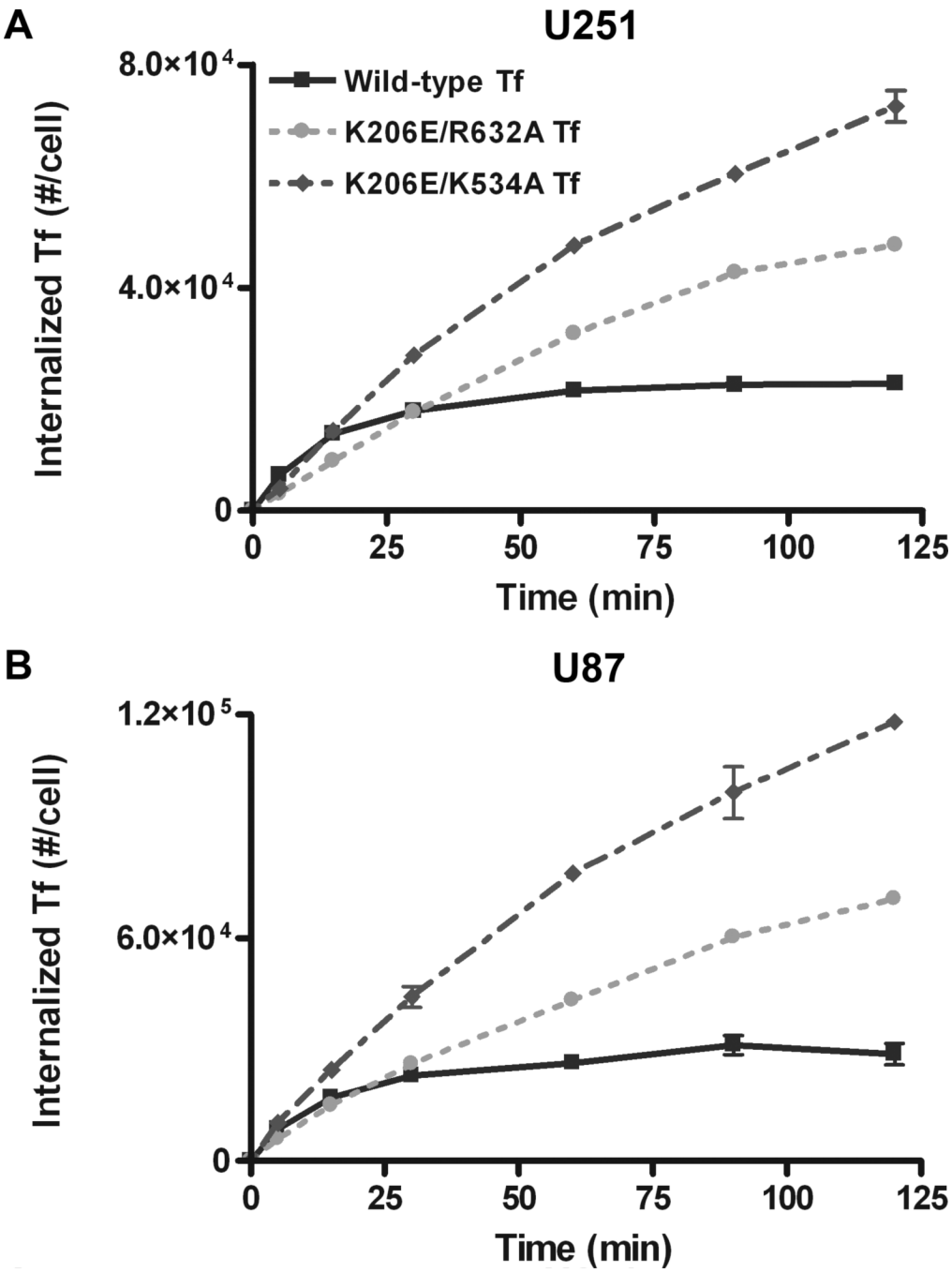

Figure 1.
Representative Tf/TfR cellular trafficking results for (A) U251 and (B) U87 glioma cells. Error bars represent standard deviations from an average of three measurements.

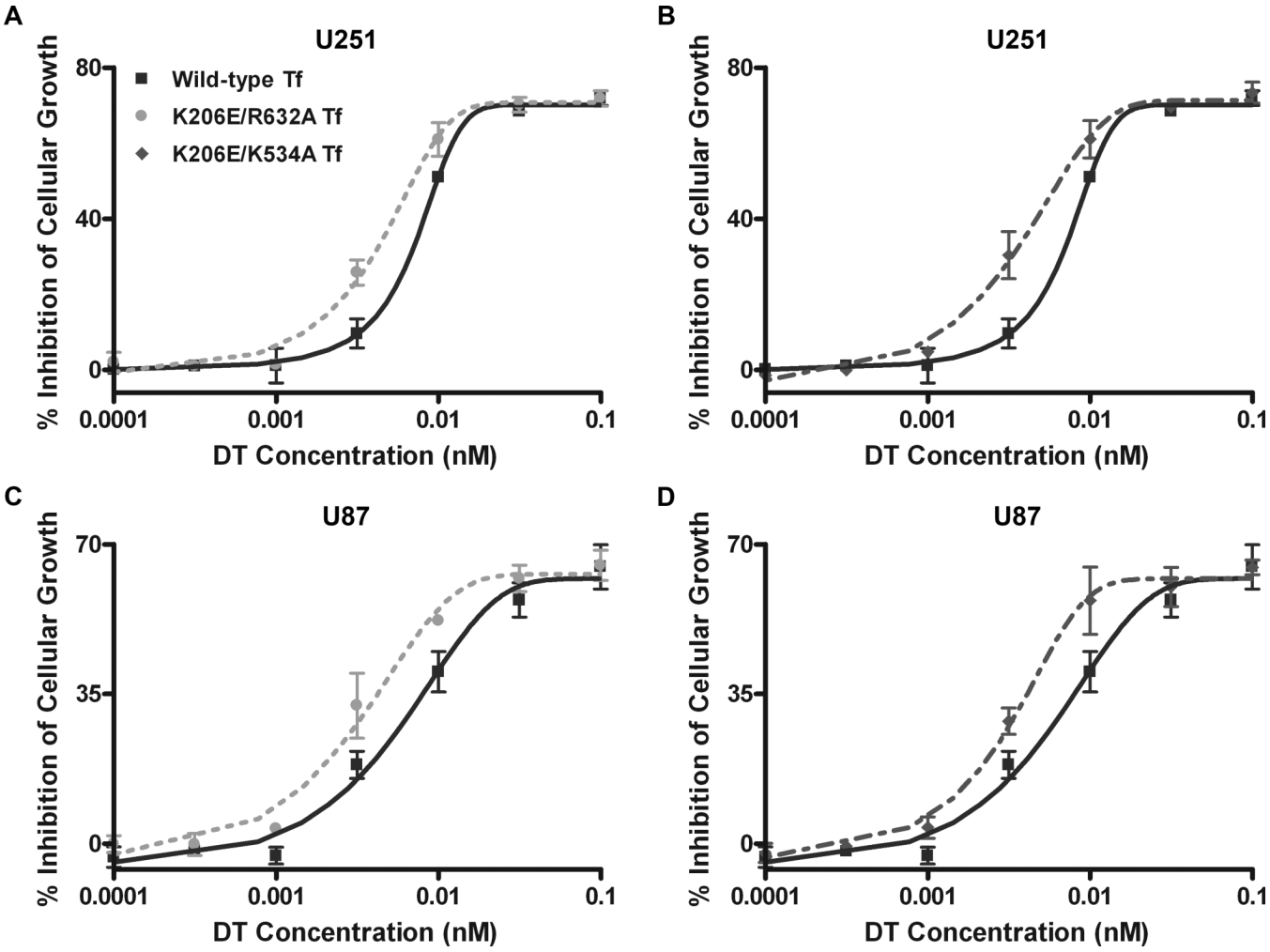

Figure 2.

In vitro cytotoxicity comparisons for DT conjugates. Error bars represent standard deviations from an average of three experiments. Wild-type Tf vs. (A) K206E/R632A Tf and (B) K206E/K534A Tf in U251 cells. Wild-type Tf vs. (C) K206E/R632A Tf and (D) K206E/K534A Tf in U87 cells.

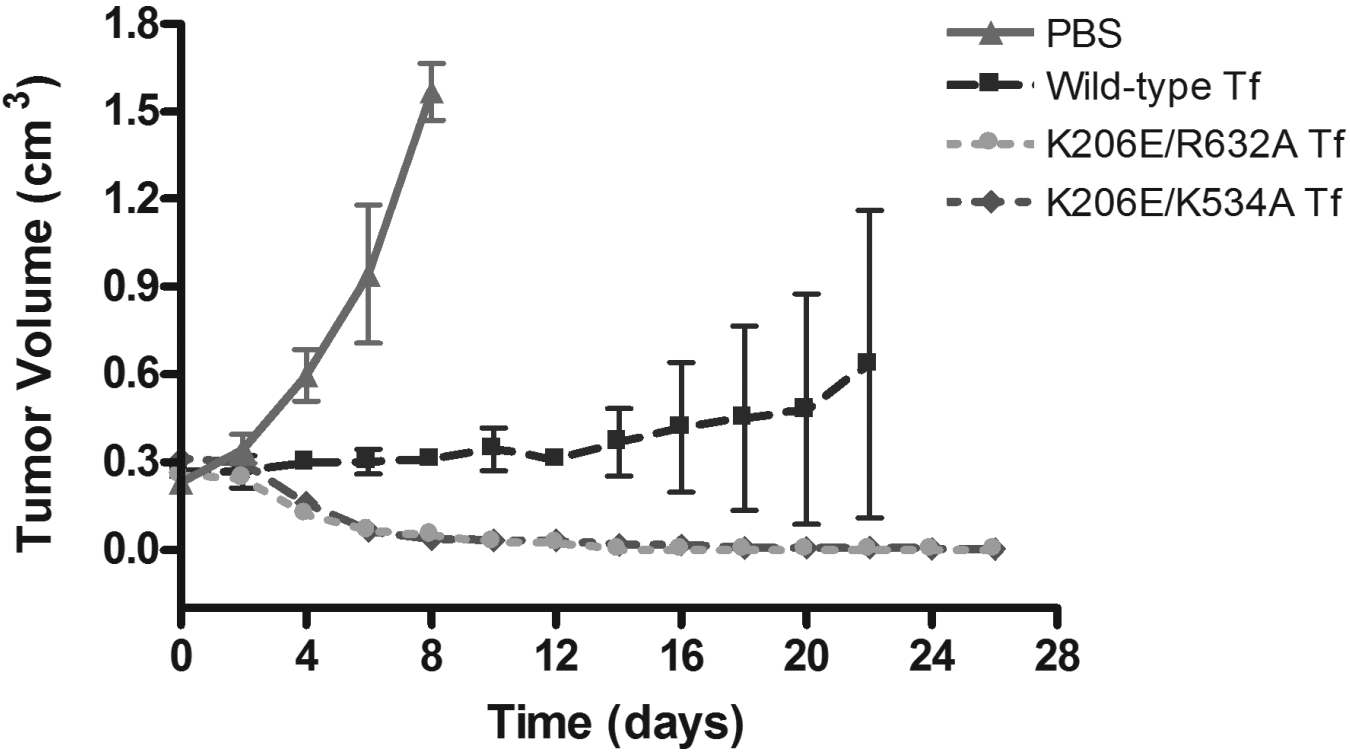

Figure 3.
Tumor volume data for female nude mice with established U87:*EGFRvIII* glioma flank tumors treated with PBS control or DT conjugates of wild-type Tf, K206E/R632A Tf, or K206E/K534A Tf. Error bars represents the standard error of the tumor volume evaluated from an average of four tumors within each treatment group.

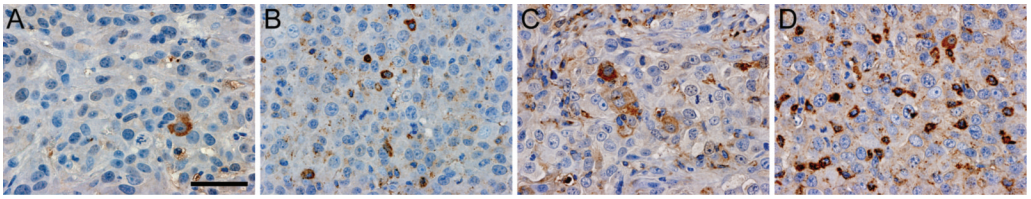

Figure 4.

Immunostaining for cleaved caspase-3 (reddish brown regions) in U87:*EGFRvIII* xenograft sections from mice treated with (A) PBS control, or DT conjugates of (B) wild-type Tf, (C) K206E/K534A Tf, or (D) K206E/R632A Tf. The blue regions represent nuclei counterstained with hematoxylin. Scale bar = 50 μm.